Ti-MWW Catalysts for Propylene Oxide Production

Alvear, Matias; Schmidt, Christoph; Reinsdorf, Ole; Lebron-Rodrigez, Edgard; Al Abdulghani, Abdullah; Hermans, Ive; Peurla, Markus; Lastusaari, Mika; Eränen, Kari; Murzin, Dmitry Yu; Kumar, Narendra; Salmi, Tapio

Published in:
Catalysis Letters

DOI:
10.1007/s10562-023-04350-x

Published: 01/03/2024

Document Version
Final published version

Document License
CC BY

Catalysis Letters (2024) 154:834–845
https://doi.org/10.1007/s10562-023-04350-x

Ti-MWW Catalysts for Propylene Oxide Production: Influence of Si/Ti Ratio and Calcination Conditions

Matias Alvear[1] · Christoph Schmidt[1] · Ole Reinsdorf[1] · Edgard Lebron-Rodrigez[2] · Abdullah Al Abdulghani[3] · Ive Hermans[2,3] · Markus Peurla[4] · Mika Lastusaari[5] · Kari Eränen[1] · Dmitry Yu. Murzin[1] · Narendra Kumar[1] · Tapio Salmi[1]

Received: 22 January 2023 / Accepted: 17 April 2023 / Published online: 27 April 2023

Abstract

Titanium silicates of MWW structures with different Si/Ti ratios were prepared via hydrothermal synthesis using piperidine as the structure directing agent and boric acid as the crystallization agent. All the syntheses resulted in highly crystalline materials independent of the Si/Ti ratio. The observed morphology showed MWW-like well-defined thin hexagonal platelets. The synthesized Ti-MWW materials exhibited higher surface areas and partial meso-porosity compared to the commercial TS-1 catalyst. The coordination of the Ti-species was investigated by UV–vis- and IR-spectroscopy. The MWW titanium silicates were tested for the catalytic performance in the epoxidation of propylene in a laboratory-scale trickle bed reactor to compare their clear different physico-chemical properties with the commercial TS-1. The synthesized Ti-MWW materials showed significantly higher catalytic activities, up to 3.5 times, using acetonitrile as the solvent and enhanced epoxide selectivities partially up to 100% in methanol unlike TS-1. The effect of the Ti content in the MWW and the calcination conditions were investigated in propylene epoxidation, revealing the beneficial effect of a lower calcination temperature and an increased Ti content on the activity. The catalytic results were correlated with the physico-chemical properties of the synthesized materials.

Graphical Abstract

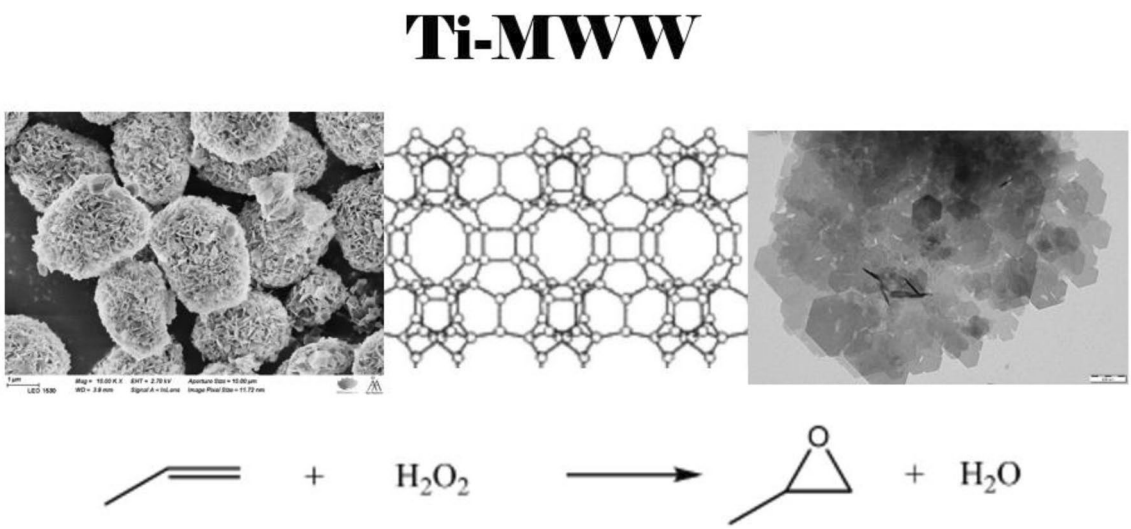

Keywords Propene · Epoxidation · Titanium-based catalyst

Extended author information available on the last page of the article

1 Introduction

Zeolites have become one of the most important catalytic materials since the breakthrough in the hydrothermal synthesis of new aluminosilicate classes in the 1970's by Mobil Oil [1]. Due to their special properties, i.e. the presence of acidic centers and well-defined topology resulting in a microporous structure, zeolites are used in a broad range of advanced applications, including oil refining, petrochemistry and detergency [2]. The structures of aluminosilicates can be tuned by using various structure directing agents and preparation methods to achieve the required properties, such as the pore size and acidity strength [3]. Initially, the scientific and industrial interests were mainly focused on aluminosilicates. However, with the years the research on the substitution of aluminium in the zeolite structure has become more prominent. A new class of heteroatom zeolites have been developed containing different metals (As, Ga, Fe, Ge, Sn, Zr, etc.) replacing partially or completely the aluminium in the framework [4]. The incorporation of titanium in the zeolite structures such as ZSM-5 MFI has also been reported [5]. The discovery of TS-1 in 1983 by Taramasso et al. was one of the breakthroughs in the research on zeolites [5]. It was found that TS-1 is highly applicable for the activation of hydrogen peroxide, being therefore a very suitable catalyst for several oxidation reactions for aliphatic and aromatic hydrocarbons [6]. The TS-1 catalyst became a game changer in the epoxidation propylene. Propylene oxide is an important chemical intermediate for the production many basic chemicals such as polyether polyols, propene glycols and propene glycol ethers [7]. In the past, propylene oxide was obtained by the highly toxic and corrosive chlorohydrin process to achieve a reasonable selectivity. Another industrial route was the oxirane process, where *in-situ* generated organic hydroperoxide reacts with propene. This process is extremely harmful, due to the reactive *tert*-butyl hydroperoxide formed during the reaction. Hence, the hydrogen peroxide propylene oxide (HPPO) process is an environmentally friendly alternative route, because hydrogen peroxide is directly used as the oxidant. Hydrogen peroxide is known to be a green and strong oxidant, being biodegradable and widely used in pulp and paper industry as a bleaching agent [8] between others. During the epoxidation, water is produced as a stochiometric co-product, which is one of the green advantages compared to organic oxidants. Currently the HPPO process is applied with methanol as the solvent, and a high selectivity of propylene oxide can be achieved. Nevertheless, under the process conditions methanol and water can undergo a consecutive reaction with the epoxide giving several side products, such as 1-methoxy-2-propanol or propylene glycol [9]. The undesired side products can form with the epoxide an azeotropic mixture from which the desired product is difficult to remove. To avoid the undesired consecutive reactions, the HPPO process can be carried out with acetonitrile as solvent [10]. There, a 100% selectivity can be achieved but the conversion is very low in this reaction system due to the hydrophobicity of the TS-1 catalyst. Several different Ti-zeolites, such as Ti-Beta, Ti-MOR, Ti-MCM-68, Ti-MWW, TS-1 and -2 etc., have been investigated [11]. Among the different materials, Ti-MWW displayed the highest selectivity but the activity still can be improved.

The MWW zeolites exhibit medium-size pores and large supercages with inner free diameters of 7.1 Å [12]. MWW, displays two sets of independent ten-member ring pore channels, synthesized from a layered precursor through condensation. The MWW zeolites can be modified via delamination [13], pillaring [14], among others [11]. In case of Ti-MWW, the material displays a higher activity in acetonitrile as the reaction solvent, because the ring-opening side reactions are avoided, whereas they play a role in alcohol solvents. The biggest difference between TS-1 and Ti-MWW as titanium silicates is the hydrophobicity. TS-1 (Ti-MFI) is highly hydrophobic, while Ti-MWW is highly hydrophilic [15].

In order to increase the activity a new approach is reported in the present study by using Ti-MWW catalysts with varying Si/Ti ratios and different calcination conditions, which outperform the commercial TS-1 catalyst and achieve a higher conversion retaining 100% selectivity. The results demonstrate a new opportunity to upgrade the hydrogen peroxide propylene oxide (HPPO) process towards a more sustainable industry.

2 Materials and Methods

2.1 Materials

Ti-MWW catalyst was synthesized using fumed silica CAB-O-SIL® (CABOT GmbH), tetrabutyl orthotitanate (TBOT) (Sigma-Aldrich, 97%), boric acid (Merck, P.A.) as a crystallization agent, piperidine (PI) (Sigma-Aldrich, 99%) as a template while deionised water was utilized as a solvent. The chemicals were used without additional purification. In addition to the synthesised catalysts, commercial TS-1 (ACS Materials) was used as a reference. In the catalytic experiments, sieved quartz sand > 125 µm (Supelco) was used to fill the reactor above and below the catalyst bed. The reactants, propene (Linde, 99.5%) and H_2O_2 (Fisher Chemical, > 30% w/v) were dissolved in either methanol (Sigma-Aldrich, ≥ 99%) or acetonitrile (Sigma-Aldrich, ≥ 99%). Nitrogen was used as a carrier gas (Woikoski, 99.999%).

2.2 Catalyst Preparation

The Ti-MWW catalyst synthesis was carried out following the reported procedure of Wu et al. [16] with some modifications. In a typical synthesis, PI (182.5 g) was dissolved in deionised water (500 mL). The obtained solution was equally divided in two separated solutions. To the first solution, TBOT (10.8 g) was added under vigorous stirring while boric acid was added to the second (124.2 g). After 30 min of stirring, silica (45 g in each solution) was gradually added into the TBOT solution and boric acid solutions. After 1 h of stirring, both gels were merged and underwent another 1.5 h of stirring. The composition of the reactive gel was 1.0 SiO_2: 0.02 TiO_2: 0.67 B_2O_3: 1.4 PI: 19 H_2O with the Si/Ti ratio equal to 50. The gel was hydrothermally crystallized in three steps at 403, 423 and 443 K. The first two steps were kept for one day while the latter step lasted for five days. The crystallisation was performed at the stirring rate of 50 rpm. The obtained gel was filtered, washed and dried overnight. The Ti-MWW precursor was refluxed in a 6 M HNO_3 aqueous solution at 373 K for 24 h (20 ml per 1 g precursor) to remove the template molecules, framework boron, and extra-framework Ti species. The product was filtered, washed and dried overnight at 373 K. The material was calcined stepwise to 803 K and remained for 6 h to produce the final Ti-MWW catalyst. The procedure was repeated for the synthesis of other titanium silicates with different ratios of the Si- and Ti-precusors and calcination conditions, while keeping the ratio Si:B_2O_3:PI:H_2O the same. Synthesised catalysts are listed with the nomenclature, the ratio of Si- and Ti-precusors and calcination conditions in Table 1.

2.3 Characterisation Methods

The physico-chemical properties of the synthesized Ti-MWW catalysts were characterized using several characterization methods. The morphological features such as texture and shape of the crystals were studied using scanning electron microscopy (SEM. Zeiss Leo Gemini 1530). Transmission electron microscopy (TEM, JEOL JEM-1400Plus) was used to measure the crystal size. The obtained images were processed and analysed by the software ImageJ to determine the crystal size of Ti-MWW catalyst. Elemental analysis was performed with ICP-OES (Agilent 5110 ICP-OES). The absorbances of silicon, aluminum and titanium were measured with the radiation sources at wavelengths 288.2, 396.2 and 334.9 nm, respectively. The elemental compositions were calculated using calibration curves generated from known solutions. The catalyst structure, phase purity and crystallinity was investigated by powder X-ray diffraction (XRD) characterization using a PANalytical Empyrean diffractometer with a five-axis goniometer. The incident beam optics consisted of Bragg–Brentano HD X-ray mirror, fixed 1/4° divergence slit, 10 mm mask, 0.04 rad soller slit and 1° antiscatter slit. The diffracted beam optics consisted of 7.5 mm divergence slit, 0.04 rad soller slit and PIXcel detector array. The used X-ray tube was Empyrean Cu LFF. The X-ray radiation was filtered to include only Cu $K_{\alpha1}$ and Cu $K_{\alpha2}$ components. The results were analyzed with MAUD (Material Analysis Using Diffraction) analysis software [17]. The instrumental broadening was evaluated with a Si standard sample. The results were obtained with 2θ scan range from 5° to 120°.

The surface area, pore size distribution, pore volume and adsorption–desorption isotherms were obtained by nitrogen physisorption (Micrometrics 3Flex-3500) using the Dubinin–Radushkevich method for calculating the specific surface area and density functional theory for determination of the pore volume and size distribution. Before the measurements, the samples were exposed to *ex-situ* degassing, where the samples were treated under vacuum at 180 °C for 24 h. The acidities of the synthesised materials were measured by temperature programmed desorption (TPD) using ammonia as the probe molecule. The samples were pretreated with the following programme: approaching 500 °C with a heating rate of 25 K/min and keeping the temperature for 60 min and He flow of 30 ml/min, then cooling down to 100 °C and then switching a gas mixture comprising 7.5% NH_3/He for 30 min. The sample was flushed with He for 60 min and cooled down to 50 °C. The target temperature for desorption was set to 600 °C with a heating rate of 10 K/min. The target temperature were kept for 20 min. The outlet gases were monitored by a thermal conductivity detector (TCD) to analyse the absorbed NH_3. Furthermore, the Ti-MWW materials were investigated on their coordination and chemical bonds via infrared spectroscopy (IR) (Mattson ATI Genesis FTIR Spectrometer) and diffuse reflectance UV–vis (UV–vis DRS). The spectra were recorded after evacuation for 2 h at 350 °C (the vacuum level and the ramp rate of 10^{-2} Torr and 10 oC/min, respectively). After the sample

Table 1 Synthesis of Ti-MWW with the varying gel composition and calcination condition

Catalyst	Ratio Si:Ti (Atomic Si/Ti ratio)	Calcination condition
Ti-MWW-1.6-530-6	1.0:0.02 (50)	803 K, 6 h
Ti-MWW-1.6-550-6	1.0:0.02 (50)	823 K, 6 h
Ti-MWW-3-530-6	1.0:0.04 (25)	803 K, 6 h
Ti-MWW-3-530-10	1.0:0.04 (25)	803 K, 10 h
Ti-MWW-3-550-6	1.0:0.04 (25)	823 K, 6 h
Ti-MWW-4.5-530-6	1.0:0.053 (19)	803 K, 6 h
Ti-MWW-4.5-550-6	1.0:0.053 (19)	823 K, 6 h
Ti-MWW-6-530-6	1.0:0.083 (12)	803 K, 6 h
Ti-MWW-6-550-6	1.0:0.083 (12)	823 K, 6 h

was treated, it was transferred to a glovebox ($H_2O < 1$ ppm and $O_2 < 1$ ppm) and UV–vis analyses were performed thereafter. For the measurements, a Maya2000 Pro UV–vis Spectrophotometer (Ocean Optics) equipped with a deuterium/halogen light source (DH-200-BAL from Mikropack) was employed. $BaSO_4$ (99.9%, Sigma-Aldrich) was used as the 100% reflectance standard and as a matrix, with the spectrometer operated in the diffuse reflectance mode. A second measurement was conducted with an Avantes Avaspec HS-TEC CCD spectrometer through an Avantes FC-UV600-1-SR fiber optic cable. The light source was an Avantes Ava-Light-DHc that employs deuterium and halogen lamps. An Edinburgh Instruments BaSO4 disc was used as the white reference. The obtained spectra were smoothed by using the Savitzky–Golay method and plotted as absorbance.

2.4 Experimental Setup

Epoxidation experiments of propene were performed in a tailor-made trickle-bed reactor (I.D. 15 mm, length 340 mm). The reactor tube was surrounded by a copper coil to maintain the desired temperature. The flowsheet of the experimental setup is illustrated on Fig. 1.

The gas flow was fed by a calibrated mass flow controller (MFC) (Brooks instruments) while the liquid flow was controlled by high-performance liquid chromatography pump (Agilent 1100 Series). The pressure was kept on a constant level by a pressure controller (U3L Ultra Low Flow Back Pressure Regulator). A three neck-round flask was used for the separation of the liquid phase from the gas phase. A condenser was utilised for recovering the gaseous solvent. The temperature of the coolant was set to − 5 °C.

The chemical analysis was conducted online for the gas phase by gas chromatograph (GC) (Agilent 6890N G1540N) with a capillary column (Plot U and molsieve) and for the liquid phase offline. The column length was 60 m and the diameter was 530 µm and active phase thickness of 20 µm was operated isothermically at 185 °C. The gases (propene, propylene oxide and nitrogen) were calibrated by sampling each gas 10 times. For the liquid phase, the solution of the components (propylene oxide, propylene glycol, and 1-methoxy-2-propanol) were analysed at 0.625, 1.25, 2.5 and 5 wt%. The analysis error was found to be ca. 1%–2%. The concentration of H_2O_2 in the reactant solution was determined before each experiment by titration with $Ce(SO_4)_2$ using ferroin as the indicator.

2.5 Catalytic Experiments

For the epoxidation experiments, a layer of inert quartz sand was filled in the reactor in such a way that the catalyst bed was located in the middle part of the tube. The catalyst (150 mg) was diluted with quartz sand (2 g) and placed between quartz wool in the middle of the reactor tube. Above the catalytic layer, a second layer of quartz sand was filled to ensure efficient mixing of the reactants and the absorption of the gases in the liquid phase. In a typical experiment, an equimolar gas mixture flow of propene and nitrogen was set to 0.446 mmol/min and the target pressure was 4.5 bar. The reactor was heated to 45 °C. After reaching the desired pressure, the liquid flow of 0.5 ml/min was turned on. The liquid phase contained of 2 wt% H_2O_2 in methanol or acetonitrile. The flow of the gases and the liquid phase were selected in such a way that the reactor was operated in a trickle flow regime. According previous studies [9], the system reached the steady state after 2.5 h. To confirm the steady state, samples were taken after 4, 6 and 8 h for determining conversion and selectivity. For changing the solvent, the new solvent was fed into the reactor until no leftovers of the previous solvent could be seen in the GC.

The propene conversion was defined as

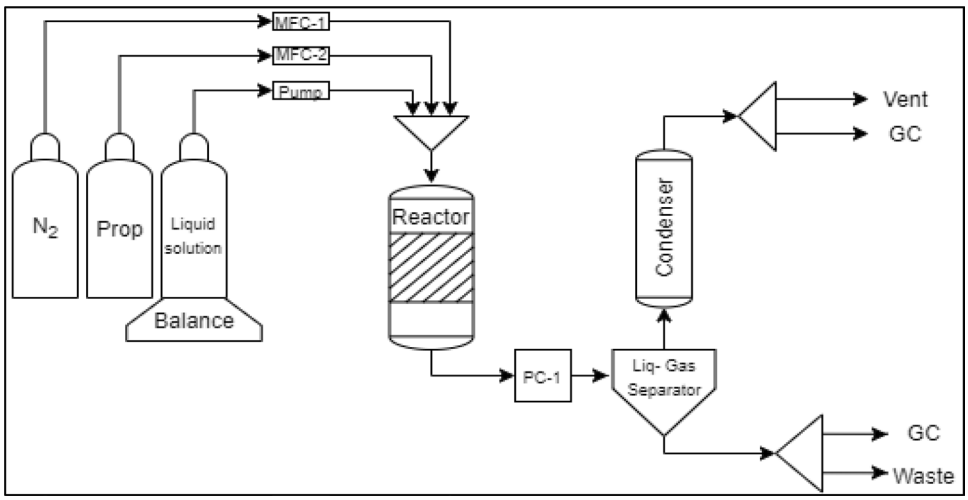

Fig. 1 Experimental setup for propene epoxidation

$$X(\%) = \frac{\dot{n}_{in} - \dot{n}_{out}}{\dot{n}_{in}} \times 100 = \frac{c_{in}\dot{V}_{in} - c_{out}\dot{V}_{out}}{c_{in}\dot{V}_{in}} \times 100 \quad (1)$$

where the indices *in* and *out* are denoted as inlet and outlet, while the variables $\dot{n}$, c and $\dot{V}$ are the molar flow, concentration and the volumetric flow, respectively. The propylene oxide selectivity was calculated with the equation

$$S(\%) = \frac{c_{\mathrm{out_{PO}}}\dot{V}_{\mathrm{out}}}{c_{\mathrm{in_{propene}}}\dot{V}_{\mathrm{in}} - c_{\mathrm{out_{propene}}}\dot{V}_{\mathrm{out}}} \times 100 \quad (2)$$

where the subscript PO refers to the product propylene oxide.

Turnover frequency (TOF) was defined as

$$TOF\left(s^{-1}\right) = \frac{\left[\dot{n}_{\mathrm{in}} - \dot{n}_{\mathrm{out}}\right]_{\mathrm{propene}}}{\text{mol of titanium in the catalyst bed}} \quad (3)$$

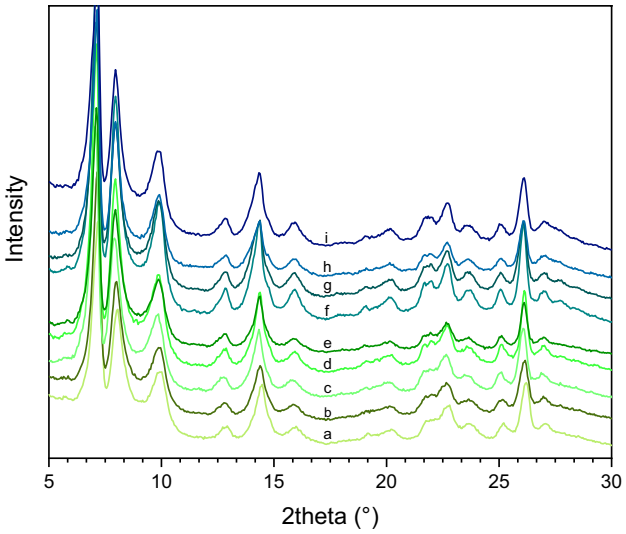

Fig. 2 XRD patterns of synthesised Ti-MWW structures: (a) -1.6-530-6, (b) -1.6-550-6, (c) -3-530-10, (d) -3-530-6, (e) -3-550-6, (f) -4.5-530-6, (g) -4.5-550-6, (h) -6-530-6 and (i) -6-550-6

3 Results and Discussion

3.1 Catalyst Characterisation

The hydrothermal synthesis resulted in a highly crystalline Ti-MWW catalyst, whereas boric acid acts as a structure-supporting agent to stabilise the structure in absence of alkali-cations and to incorporate a high content of Ti. XRD confirmed crystallinity of all the synthesised materials [16].

The XRD patterns of the synthesised Ti-MWW structures are shown in Fig. 2. All samples had with the typical MWW signals obtainable from the database, thus confirming the topology. Furthermore, the crystallinity judging from the shape of the reflexes remains high. The Ti-MWW structure is mainly characterised by the intralayer orientation in *c*-direction and the sheets in the *ab*-plane. The signals at $2\Theta = 7.1°$ (100), 25.1° (220) and 26.2° (310) can be assigned to the layered structure of the stacked sheets [18]. All other signals originate from the typical platelets in the *ab*-plane. However, a small amount of impurities is present in the samples, suppressing the reflexes in the low region of 2θ signals, like at 19.1°, which can be only observed in one sample (Fig. 2f).

The images, obtained by TEM, confirmed the layered structure of the single platelets. On The micrographs, the platelets are visible as their orientation is along the ab-plane according to Fig. 3a. The upright standing platelets reveal the stepwise changing thickness. Particularly towards the edges a splitting of the single platelets is observed, clearly indicating laminar morphology of the material. The platelets were 50–300 nm in length and 3–45 nm in thickness. Figure 3a is representative for all Ti-MWWs materials. No visible effects of the calcination temperature or duration could be found. However, for a higher Ti content, non-laminated 3D structures were present to a certain extent (Fig. 3b) but no agglomerate sheets, where the crystal growth took place in one orientation only, was observed (Fig. 3c). This is produced by the crystallization on the walls and corners of the inner teflon vessel in the rotating autoclave. In contrast, the smaller better defined crystals are obtained, which are mainly created due to the dynamic crystallization from the constantly rotating autoclave and the motion of the reacting gel [19]. Furthermore, in some places occasional an additional growth of the titanium silicate in the typical crystal shape was observed, which appears as blossoms at the outer shell of the agglomerated platelets (Fig. 3d).

The scanning electron micrographs of Ti-MWW exhibited the presence of typical platelet shaped crystals of MWW type microporous materials. The morphological features of the Ti-MWW was clearly observed in all the samples studied, since the surface of the material and not the transmission was imaged. Some findings from TEM images are supported by SEM micrographs displayed in Fig. 4. The platelets are present as spherically shaped agglomerates with diameters of 2–4 µm. Moreover, the mentioned non-laminated 3D crystals with a hexagonal shape can be seen in Fig. 4a. At a higher magnification, the characteristic well-defined hexagonal sheets of the synthesised material are visible. At a lower magnification, it can be found at this point of the synthesis and under these conditions partially intact and partially broken larger spheres with the diameter of 15–35 µm. From the micrograph displayed in Fig. 4c, it is inferred that larger particles break apart forming smaller agglomerates, indicated by cracking of the hollow particles. Hereby the fraction of the small agglomerates is significantly larger than the

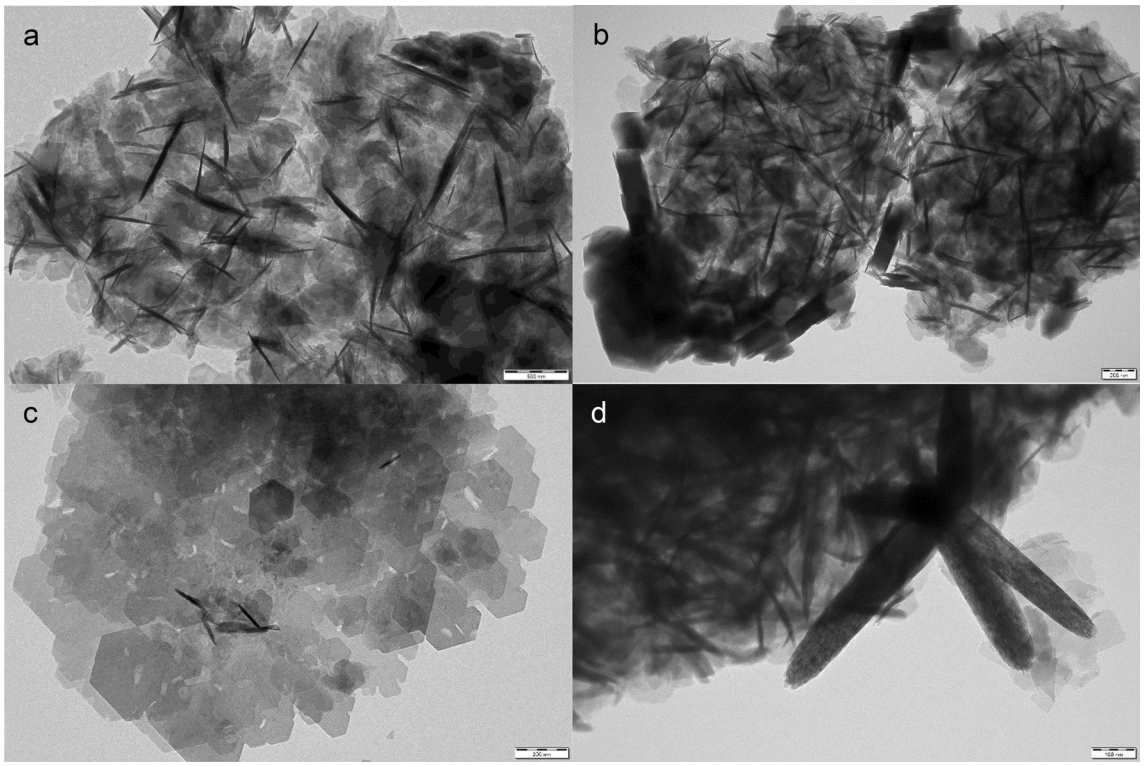

Fig. 3 Transmission electron micrographs of Ti-MWW-1.6-550-6 (**a**) and Ti-MWW-3–530-6 (**b**), (**c**) and (**d**)

bigger particles. As already observed from the TEM images, the shown images are representative for all the synthesised materials. Neither the duration nor the temperature of the calcination procedure affected the morphology. As the ratio of Si/Ti is changed towards a higher Ti content, the contribution of the planar shaped crystals increases compared to the agglomerates of single platelets. This fact indicates a higher mechanical stability of the titanium silicates, despite using the same dynamic crystallisation process. This phenomenon was visible especially for Ti-MWW-4.5 and -6 samples and only in small amounts in TiMWW-3 materials. These crystal shapes were not observed in the Ti-MWW-1.6 silicates.

Nitrogen physisorption was carried out to investigate the textural properties such as surface area, pore volume, pore size distributions and adsorption–desorption isotherms of the Ti-MWWs materials. These results were compared with the properties of the commercial TS-1 titanium silicate. High surface areas were found for the synthesized catalysts, ranging from 420 to 480 m^2/g. An exception among the prepared catalysts was Ti-MWW-3-550-6 with 371 m^2/g, the decrease in the surface area can be attributed to the distortion of the structure of this catalyst. However, all the Ti-MWW materials displayed higher specific surface areas in comparison to TS-1 being 319 m^2/g. Moreover, the prepared titanium silicates had ca. two-fold higher pore volumes related to the commercial reference material. A closer look on the porosity reveals that additional meso-pores are contributing to the micro-porosity in case for Ti-MWWs. In contrast, TS-1 mainly exhibits micro-porosity. Since the Ti-MWW and TS-1 crystals themselves contain micro-pore channels only, the meso-porosity originates from a secondary structure formed by the calcination of the 2D MWW precursor, leading to a partial condensation of the single sheets. As Fig. 4b shows, the agglomerates build cavities between the single sheets, thus creating the meso-porosity. The second reason for a higher pore volume can be found in their different topologies. The framework of the MWW structure contains large internal supercages, which are not present in the MFI framework of TS-1[20]. The micro-porous volumes of the synthesised titanium silicates are up to 40% higher than determined for TS-1.

It was found that the different calcination processes influence the formation of the pores (Table 2), which is caused by the removal of the organic compound tetrabutyl orthotitanate (TBOT) and crystallization agent piperidine (PI). Furthermore, it was observed that the calcination process at 550 °C results in a decrease of micro- and particular mesopores regarding to the calcination process at 530 °C for the entire series (Ti-MWW-x-530/550-6). A possible explanation is the higher degree of condensation of the framework with a higher calcination temperature, which leads to the closure of the pores. It was also observed that the

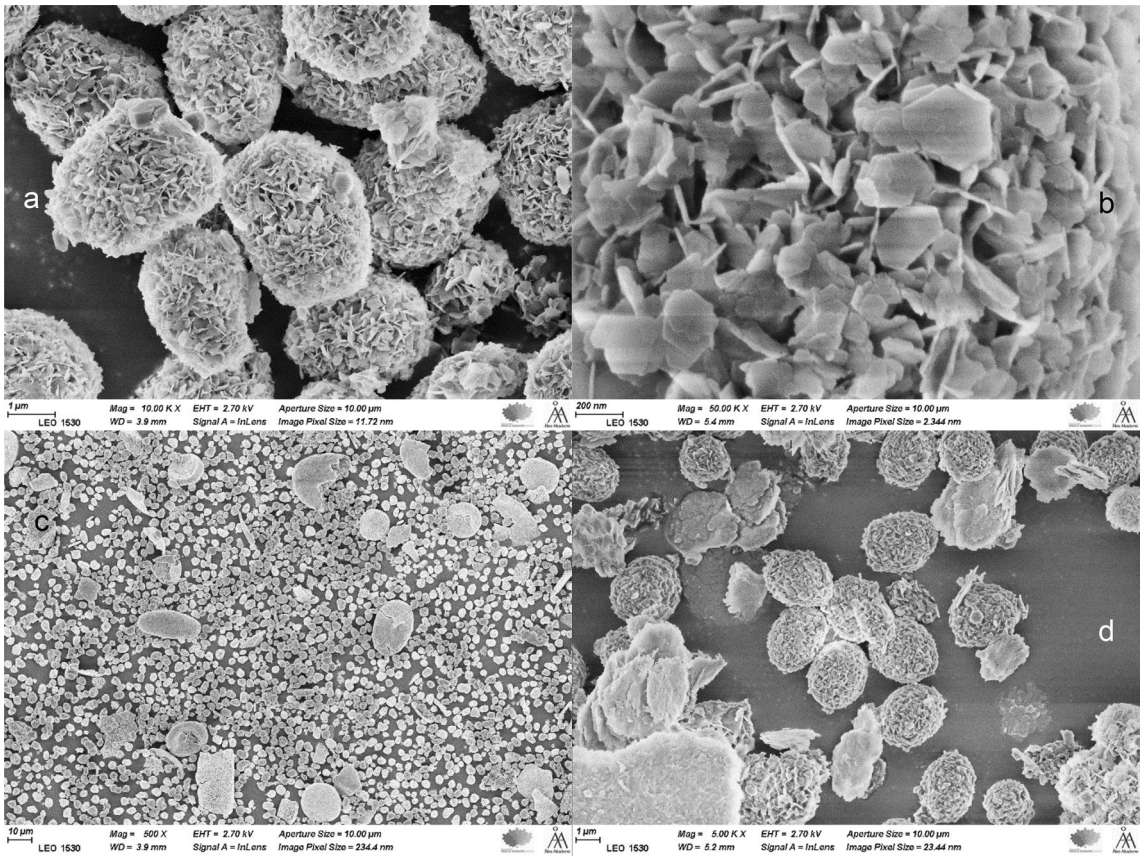

Fig. 4 Scanning electron micrographs of **a** Ti-MWW-3-550-6, **b** Ti-MWW-6-530-6, **c** Ti-MWW-3-530-6, **d** Ti-MWW-4.5–530-6

Table 2 Textural properties of Ti-MWW, TS-1 catalysts and the element analysis of Si and Ti

Catalyst	SSA[a]	V_{pores} [cm^3/g]			d_{pores}[b]	Si	Ti	Atomic Si/Ti Ratio
	[m^2/g]	V_{micro}	V_{meso}	V_{tot}	[nm]	[wt%]		Nominal
Ti-MWW-1.6-530-6	481	0.21	0.19	0.40	0.66	46.3	1.2	50
Ti-MWW-1.6-550-6	434	0.19	0.13	0.32	0.65	–	–	–
Ti-MWW-3-530-6	464	0.21	0.27	0.48	0.66	48.1	1.7	25
Ti-MWW-3-530-10	424	0.17	0.32	0.49	0.65	–	–	–
Ti-MWW-3-550-6	371	0.16	0.25	0.41	0.66	–	–	–
Ti-MWW-4.5-530-6	459	0.20	0.28	0.49	0.66	47.5	2.6	19
Ti-MWW-4.5-550-6	423	0.19	0.21	0.40	0.66	–	–	–
Ti-MWW-6-530-6	470	0.21	0.19	0.39	0.66	48.6	4.8	12
Ti-MWW-6-550-6	449	0.20	0.18	0.38	0.66	–	–	–
TS-1	319	0.15	0.04	0.19	0.63	–	–	–

Legend: *SSA* specific surface area, V_{pores} pore volume and d_{pores} average pore size

[a]Calculated with the Dubinin–Radushkevich method

[b]Calculated with the Horvath–Kawavoe method

calcination of Ti-MWW-3 during 10 h leads to an increase of the mesopores, while the micropores decrease comparing to 6 h of calcination at 530 °C.

The two types of channel systems also result in different average pore sizes. For Ti-MWWs an almost constant value of ca. 0.66 nm was found, indicating the uniform channel system for all synthesized materials, whereas the average pore size of TS-1 is 0.63 nm. One of the main objectives of the work is to study the influence of different Ti contents in the MWW framework. For the determination of the

composition, ICP-OES was used for elemental analysis. A sample from each synthesis batch was analyzed with a theoretical (Si:Ti) ratio of 50, 25, 19 and 12. The obtained weight percentages of Si and Ti are summarized in Table 2. From these values, the calculated atomic ratios are 65.7, 47.2, 31.4 and 17.2, respectively, being higher than the nominal values. Due to the acid treatment aimed at the removal the extra framework Ti-species, which are not incorporated in the MWW structure, there is a shortage of Ti of 24–47 wt%. This loss results in defects in the structure, were confirmed by XRD, where smaller signals are poorly recognized.

Titanium silicates had been characterized as purely Lewis acid materials [21]. The acidity determination was done by ammonia TPD (Figure S2, an example of TPD spectra recorded), where the results show the important role of the Si/Ti ratio for the acidity of the material. The acidities are displayed in Fig. 5. Here, a clear decrease of the acidity from Ti-MWW-4.5 and -6 to -3 and 1.6 was found, comparing the materials, which were treated under same calcination conditions. The drop is specifically pronounced for the materials treated at 530 °C. It is evident that the materials with higher Ti contents can also contain potentially more acid sites. It is noteworthy to mention that despite a higher Si/Ti ratio of TS-1, which is ≥ 25 accordingly by the supplier, this material has an acidity lower than the Ti-MWW-6-530-6 with a ratio of 17.2. Moreover, the change of the calcination temperature had an impact in the acidity of the material, where particularly the Ti-MWW-4.5 and -6 materials with higher Ti content calcined at higher temperature possess significant a lower acidity. It is possible that at higher temperatures the condensation of tetrahedral to octahedral non-acidic Ti-species is more likely. Coordination of the Ti-species are decisive for acidic properties [22]. Unsaturated tetrahedral TiO_4 is able to accept electrons and therefore exhibits acidity, whereas on the contrary saturated TiO_6 octahedra are non-acidic [23]. Consequently, Ti-MWW-4.5 possesses a higher amount of tetrahedral coordinated Ti than Ti-MWW-6 despite a higher Ti content. These observations are coherent with the results obtained by IR-spectroscopy, illustrated in Fig. 6. The band at 960 cm^{-1} is the characteristic stretching vibration band of tetrahedral Ti-species, which are considered to be the active species in the epoxidation of olefins, at the bond Si–O–Ti[24]. The IR-spectra reveal an increase in the Ti content leads to a more intense band. However, both bands from Ti-MWW-6 display lower intensity than the ones from Ti-MWW-4.5 indicating less tetrahedral coordinated Ti-species, supporting the conclusions from the acidity measurements. An increase of the intensity is especially remarkable for Ti-MWW-1.5 and -3 materials, considering similar calcination conditions. Moreover, it was found that a lower calcination temperature of all catalysts, particular for Ti-MWW-1.6 and -3, result in a more distinct band at 960 cm^{-1}. A negative effect on the amount of tetrahedral Ti-species was also observed for a longer duration of the calcination treatment, as can be seen by comparing the spectra of Ti-MWW-3-530-6 and -10. This result is consistent with the decreasing specific surface areas and the condensation of acidic tetrahedral Ti-species with higher calcination temperature. The coordination of titanium can also be investigated with UV–vis spectroscopy. In the literature, the band at 220 nm is assigned to the tetrahedral, 260 nm to octahedral and 330 nm to anatase Ti-species in the extraframework. The displayed spectra in Fig. 7 show a peak at 230–237 nm and for a higher Ti content a broad band around 319 nm. The positions of the obtained bands in the spectra is different from other reports [11, 16, 25], however, judging from the shape of the curves the former signal can be assigned to the desired tetragonal Ti-species and the latter

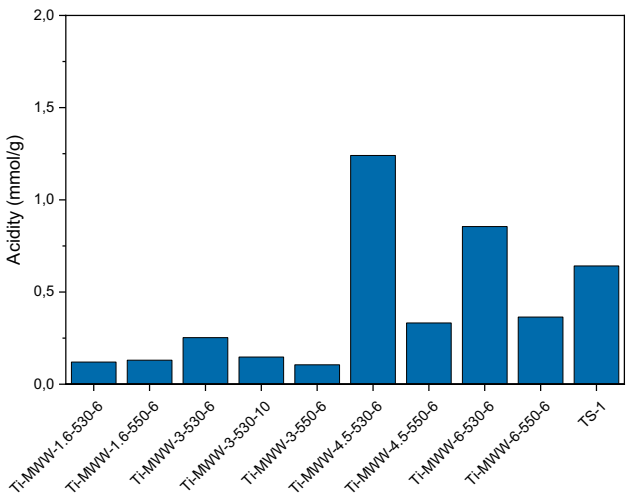

Fig. 5 Acidities of Ti-MWW materials and TS-1

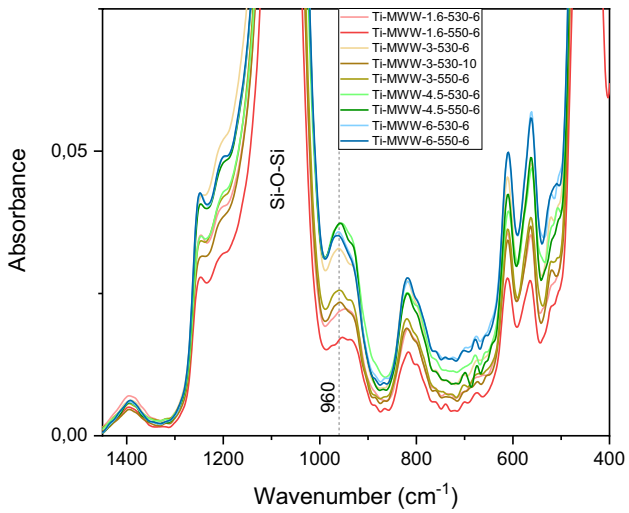

Fig. 6 IR-spectra of synthesized Ti-MWW materials

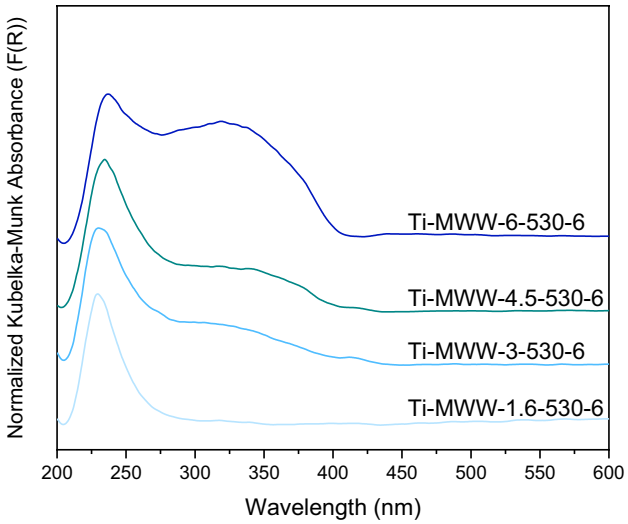

Fig. 7 Absorbance UV–vis-spectra of synthesized Ti-MWW materials

broad band at ca. 319 nm to the anatase-like species. The UV–vis spectra suggest an increase in the concentration of extra-framework titanium with the increase in the titanium loading.

The spectra reveal the increased formation of anatase-like species when the material contains more Ti, with a good agreement with the SEM images. Ti-MWW-3 and -4.5 show similar absorbance at this wavelength whereas Ti-MWW-6 displays a significate increase of the absorbance. Hence, introducing of more titanium leads to the formation of undesired anatase-like species. The result is also consistent with the IR-spectra, where Ti-MWW-6 exhibits even less absorbance at 960 cm^{-1} than Ti-MWW-4.5, despite a higher content of Ti. The recorded spectra from the UV–vis measurement are reproducible, confirmed by using second measuring instrument. The results obtained from the Avantes Avaspec HS-TEC CCD spectrometer are in the Supplement and show the spectra of the full set of the prepared catalysts.

3.2 Evaluation of Catalytic Activity and Selectivity of the Ti-MWW Catalysts in Propene Epoxidation

The catalytic results from the trickle bed experiments are displayed in Table 3. One of the most important results is the superior conversion of propene in acetonitrile, being up to 3.5 times higher for Ti-MWW catalysts compared to TS-1. The epoxide selectivity was for all the catalysts at 100%. In methanol, the opposite behaviour was found: when a larger conversion with TS-1 was achieved, the selectivity decreased. Interestingly, switching the solvent from acetonitrile to methanol displays a considerable increase of the propene conversion in case of TS-1 and a slight decrease in case of the Ti-MWW materials. This kind of behaviour has been previously reported by Tong et al. [11], where the phenomenon was explained by different adsorption strengths of the solvents on Ti-MWW. While MeCN is an aprotic solvent, MeOH is a protic one adsorbing more strongly in the channels of the MWW structure, and hindering diffusion of the reactants, which results in lower activity. However, it is still under investigation, why the conversion in methanol is significantly higher using TS-1 instead of Ti-MWW, while the opposite results were observed for acetonitrile. It is widely reported that the solvent has a strong influence on the activity and selectivity in the HPPO process, since many factors, such as the reactant solubility, the protonation ability of the solvent and the hydrophilic/hydrophobic interactions with the catalyst affect the reaction system [26], which might give a lower selectivity in methanol than in acetonitrile. Herein, TS-1 exhibits among the screened catalysts the lowest selectivity of 92.4%. All prepared Ti-MWW catalysts afforded higher selectivities and even for Ti-MWW-1.6-530-6 and Ti-MWW-3-550-6 no by-products were detected. The enhanced selectivity of the reaction in acetonitrile compared to methanol has been reported previously [27]. The use of acetonitrile as a solvent did not result in any by-products. On the other hand, a lower selectivity in

Table 3 Conversion and selectivity of the synthesised Ti-MMW and TS-1 as a reference in MeOH and MeCN as solvents

	Conversion [%]		Selectivity [%]		TOF [s^{-1}]	
	MeCN	MeOH	MeCN	MeOH	MeCN	MeOH
Ti-MWW-1.6-530-6	5.0	3.4	100	100	0.30	0.20
Ti-MWW-1.6-550-6	4.9	2.7	100	95.0	0.29	0.16
Ti-MWW-3-530-6	7.3	4.4	100	94.8	0.30	0.18
Ti-MWW-3-530-10	7.1	4.4	100	98.8	0.29	0.18
Ti-MWW-3-550-6	5.1	2.6	100	100	0.21	0.11
Ti-MWW-4.5-530-6	16.3	8.2	100	96.0	0.45	0.23
Ti-MWW-4.5-550-6	15.5	8.9	100	94.8	0.43	0.25
Ti-MWW-6-530-6	17.6	10.0	100	95.1	0.26	0.15
Ti-MWW-6-550-6	14.9	8.9	100	96.2	0.22	0.13
TS-1	4.8	23.2	100	92.4	0.10	0.47

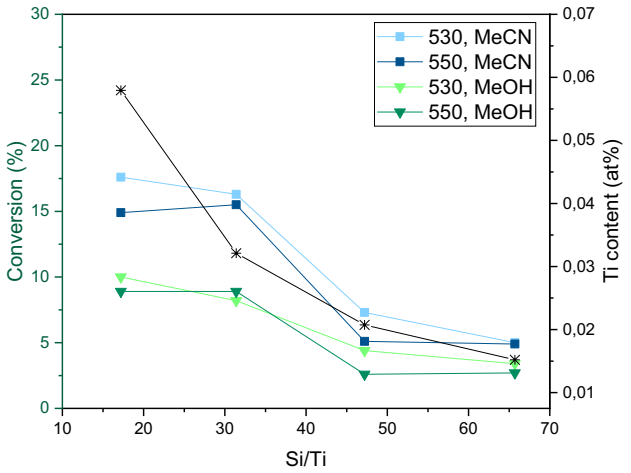

Fig. 8 Conversion of propene in methanol (triangle, green) and acetonitrile (square, blue) vs. the Si/Ti ratio of Ti-MWWs for calcination temperatures 530 (bright) and 550 °C (dark) combined with the Ti content (asterisk) vs. the Si/Ti ratio

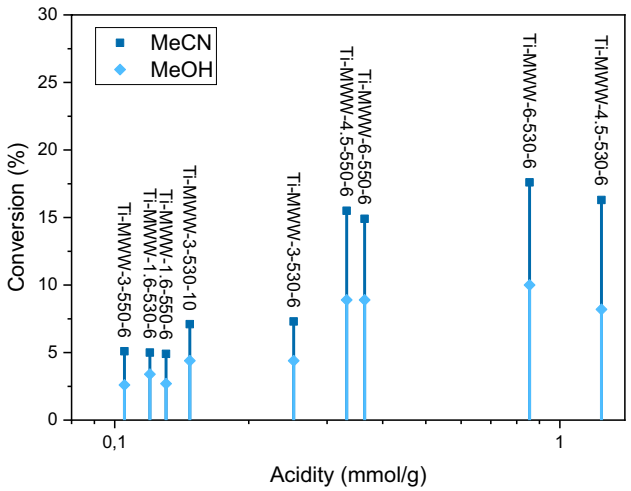

Fig. 9 Conversion of propene in methanol (diamond, light blue) and acetonitrile (square, blue) vs. the acidity of Ti-MWW catalysts

methanol is caused by a consecutive reaction of the solvent itself with the epoxide because a nucleophile attack leads to ring opening. Contrary to methanol, acetonitrile is not able to perform a nucleophilic addition of the epoxide ring. Another factor for the lower selectivity in methanol in the presence of TS-1 is the significantly higher activity. To illustrate better the influence of the Si/Ti ratio on the propylene conversion, the obtained data are plotted separately in Fig. 8.

A clear effect of the composition for both solvents and both calcination temperatures was observed, with a higher conversion at a lower titanium content apart from Ti-MWW-4.5-550-6 which gave a higher or equal conversion than Ti-MWW-6-550-6 in acetonitrile compared to methanol. Notably, a sharp increase appears in the conversion from Ti-MWW-3 to Ti-MWW-4.5 especially in the presence of acetonitrile. As described above, the Si/Ti ratio affects directly the acidity of the materials. In Fig. 9, the influence of the acidity on the conversion is illustrated. Here, the increase of the propene conversion from Ti-MWW-3 to higher Ti containing catalysts is visible as in Fig. 8. Interestingly, the drastic increase of the acidity of Ti-MWW-4.5 and -6 prepared at 530 °C compared to higher calcination temperature, resulted only in a slightly increase the conversion. The comparison of the turnover frequency (TOF) of the catalyst, when considering the Ti content as active sites, suggest similar activities for the Ti-MWW-4.5 and the commercial TS-1 catalysts. The selectivities of the Ti-MWW materials is superior suggesting an improvement in the utilization of propylene. From the determination of the physico-chemical properties, the results can be correlated to the drastic increase of the acidity from Ti-MWW-3 to -4.5. All the synthesized catalysts of the Si/Ti ratio 47.2 and 65.7 resulted in comparable acidities, whereas the ratio 31.4 is around 10 times and 17.2 6.5 times higher, as shown in Fig. 5. From a sharper slope in Fig. 8, it can be deduced that the change in the acidity affects the conversion in acetonitrile more than in methanol. It can be also concluded from Fig. 8 that better performance was achieved for Ti-MWW catalysts calcined at 530 °C. A possible explanation is provided by the IR-spectra, where the 960 cm^{-1} bands are more intensive for materials calcined at 530 °C than for at 550 °C indicating a higher presence of the active tetrahedral Ti-species and thus a higher epoxidation activity. The catalytic results are in good agreement with the two Ti-containing catalysts with a lower Ti content. However, this explanation cannot be used for Ti-MWW-4.5 and -6 materials, where the bands are almost equally intense. Considering a significantly higher Ti content in the Ti-MWW-6 catalysts, it should lead to high conversions, unless there would be an acidity drop for these catalysts. Nevertheless, a minor increase of the conversion or then similar or even lower conversions were found for catalyst calcined at 530 °C and 550 °C, respectively. It can be deduced that incorporation of titanium in the framework in case of high Ti content is only partial. This was confirmed by the obtained UV–vis spectra, where the band of anatase-like Ti-species is most intensive in the Ti-MWW-6-530-6 sample. However, due to the complexity of the reaction, the catalytic behaviour cannot be ascribed to a single descriptor, such as acidity or Ti content.

4 Conclusions

Titanium silicates of the MWW topology with different Si/Ti ratios ranging 17 to 66 and calcination conditions were successfully synthesized. The physico-chemical properties of the Ti-MWW catalysts were characterized using SEM–EDS,

TEM, XRD and nitrogen physisorption methods. The Ti-MWW materials displayed a high catalytic activity in the selective epoxidation of propene to propylene oxide. The catalytic experiments in the laboratory-scale trickle bed reactor revealed an enhanced conversion in acetonitrile in the presence of Ti-MWW compared to commercial TS-1. Furthermore, it was found that the synthesized materials exhibited a higher selectivity when the reaction is performed in methanol, compared to the TS-1 catalyst. The titanium silicates with MWW topology gave, in contrary to TS-1, a higher propene conversion in acetonitrile than in methanol as the reaction medium. A positive effect was found when the calcination of the precursor was conducted at a lower temperature to increase the formation of the active tetrahedral Ti-species. An increase of the Ti content resulted mainly in a higher catalytic activity for both solvents, but also an elevation in the formation of inactive anatase species. When changing the Si/Ti ratio from 31 to 47, a decrease of the acidity was confirmed accompanied by a decrease in the propene conversion. This decrease was more significant when the reaction was carried out in acetonitrile instead of methanol. The catalytic results showed the industrial potential of the Ti-MWW. For the industrial application in the HPPO process, acetonitrile is of potential interest, because, as the complete epoxide selectivity is achieved, no by-products are produced and thus, the separation step can be avoided.

Supplementary Information The online version contains supplementary material available at https://doi.org/10.1007/s10562-023-04350-x.

Acknowledgements This research work is part of the activities financed by Academy of Finland through the Academy Professor grants 319002, 320115, 345053 (T.Salmi and M.Alvear) and partially the Fortum and Neste Foundation for the grant 20210010 (C. Schmidt). Transmission electron microscopy images were recorded at the Institute of Biomedicine, University of Turku.

Funding Open access funding provided by Åbo Akademi University (ABO).

References

1. Argauer RJ, Landolt GR. (1972) Crystalline zeolite zsm-5 and method of preparing the same. US3702886A.
2. Olson DH, Haag WO, Lago RM (1980) Chemical and physical properties of the ZSM-5 substitutional series. J Catal 61:390–396. https://doi.org/10.1016/0021-9517(80)90386-3
3. Weitkamp J (2000) Zeolites and catalysis. Solid State Ion 131:175–188. https://doi.org/10.1016/S0167-2738(00)00632-9
4. Pang T, Yang X, Yuan C, Elzatahry AA, Alghamdi A, He X et al (2021) Recent advance in synthesis and application of heteroatom zeolites. Chin Chem Lett 32:328–338. https://doi.org/10.1016/j.cclet.2020.04.018
5. Taramasso M, Perego G, Notari B. (1983) Preparation of porous crystalline synthetic material comprised of silicon and titanium oxides. US4410501A.
6. Laha SC, Kumar R (2002) Highly selective epoxidation of olefinic compounds over TS-1 and TS-2 redox molecular sieves using anhydrous urea-hydrogen peroxide as oxidizing agent. J Catal 208:339–344. https://doi.org/10.1006/jcat.2002.3582
7. Pinaeva LG, Noskov AS (2020) Prospects for the development of ethylene oxide production catalysts and processes. Pet Chem 60:1191–1206
8. Goti A, Cardona F (2008) Hydrogen peroxide in green oxidation reactions: recent catalytic processes. In: Tundo P, Esposito V (eds) Green chemical reactions. Springer, Dordrecht, pp 191–212
9. Alvear M, Eränen K, Murzin DYu, Salmi T (2021) Study of the product distribution in the epoxidation of propylene over TS-1 catalyst in a trickle-bed reactor. Ind Eng Chem Res 60:2430–2438. https://doi.org/10.1021/acs.iecr.0c06150
10. Russo V, Tesser R, Santacesaria E, Di Serio M (2013) Chemical and technical aspects of propene oxide production via hydrogen peroxide (HPPO Process). Ind Eng Chem Res 52:1168–1178. https://doi.org/10.1021/ie3023862
11. Tong W, Yin J, Ding L, Xu H, Wu P (2020) Modified Ti-MWW zeolite as a highly efficient catalyst for the cyclopentene epoxidation reaction. Front Chem. https://doi.org/10.3389/fchem.2020.585347
12. Leonowicz ME, Lawton JA, Lawton SL, Rubin MK (1979) MCM-22: a molecular sieve with two independent multidimensional channel systems. Science 1994(264):1910–1913. https://doi.org/10.1126/science.264.5167.1910
13. Wu P, Nuntasri D, Ruan J, Liu Y, He M, Fan W et al (2004) Delamination of Ti-MWW and high efficiency in epoxidation of alkenes with various molecular sizes. J Phys Chem B 108:19126–19131. https://doi.org/10.1021/jp037459a
14. Hao Q-Q, Lei C-Y, Song Y-H, Liu Z-T, Liu Z-W (2016) The delaminating and pillaring of MCM-22 for Fischer-Tropsch synthesis over cobalt. Catal Today 274:109–115. https://doi.org/10.1016/j.cattod.2016.01.042
15. Zeynep Ayla E, Patel D, Harris A, Flaherty DW (2022) Identity of the metal oxide support controls outer sphere interactions that change rates and barriers for alkene epoxidations at isolated Ti atoms. J Catal 411:167–176. https://doi.org/10.1016/j.jcat.2022.05.013
16. Wu P, Tatsumi T, Komatsu T, Yashima T (2001) A novel titanosilicate with MWW structure. I. Hydrothermal synthesis, elimination of extraframework titanium, and characterizations. J Phys Chem B 105:2897–2905. https://doi.org/10.1021/jp002816s
17. Lutterotti L (2010) Total pattern fitting for the combined size–strain–stress–texture determination in thin film diffraction. Nucl Instrum Methods Phys Res B 268:334–340. https://doi.org/10.1016/j.nimb.2009.09.053
18. Schwanke AJ, Pergher S, Díaz U, Corma A (2017) The influence of swelling agents molecular dimensions on lamellar morphology of MWW-type zeolites active for fructose conversion. Microporous Mesoporous Mater 254:17–27. https://doi.org/10.1016/j.micromeso.2016.11.007

19. Schwanke A, Pergher S (2018) Lamellar MWW-Type zeolites: toward elegant nanoporous materials. Appl Sci 8:1636. https://doi.org/10.3390/app8091636
20. Shamzhy M, Gil B, Opanasenko M, Roth WJ, Čejka J (2021) MWW and MFI frameworks as model layered zeolites: structures, transformations, properties, and activity. ACS Catal 11:2366–2396. https://doi.org/10.1021/acscatal.0c05332
21. Kumar P, Gupta JK, Muralidhar G, Rao TSRP (1998) Acidity studies on titanium silicalites-1 (TS-1) by ammonia adsorption using microcalorimetry. In: Rao TSRP, Dhar GMBT-S (eds) Recent advances in basic and applied aspects of industrial catalysis. Elsevier, Amsterdam, pp 463–721
22. Sastre G, Corma A (1999) Relation between structure and Lewis acidity of Ti-Beta and TS-1 zeolites: a quantum-chemical study. Chem Phys Lett 302:447–453. https://doi.org/10.1016/S0009-2614(99)00177-3
23. Shintaku H, Nakajima K, Kitano M, Ichikuni N, Hara M (2014) Lewis Acid Catalysis of TiO_4 Tetrahedra on Mesoporous Silica in Water. ACS Catal 4:1198–1204. https://doi.org/10.1021/cs401149n
24. Bellussi G, Rigutto MS (2001) Chapter 19 Metal ions associated to molecular sieve frameworks as catalytic sites for selective oxidation reactions. In: van Bekkum H, Flanigen EM, Jacobs PA, Jansen JCBT-S (Eds.) Introduction to Zeolite Science and Practice, Elsevier, 911–55
25. Yu Y, Wang R, Liu W, Chen Z, Liu H, Huang X et al (2021) Control of Ti active-site microenvironment in titanosilicate catalysts and its effect on oxidation pathways. Appl Catal A Gen 610:117953. https://doi.org/10.1016/j.apcata.2020.117953
26. van der Waal JC, van Bekkum H (1997) Zeolite titanium beta: A versatile epoxidation catalyst. Solvent effects. J Mol Catal A Chem 124:137–146. https://doi.org/10.1016/S1381-1169(97)00074-5
27. Song F, Liu Y, Wang L, Zhang H, He M, Wu P (2007) Highly efficient epoxidation of propylene over a novel Ti-MWW catalyst. In: Xu R, Gao Z, Chen J, Yan WBT-S, (Eds.), From Zeolites to Porous MOF Materials The 40th Anniversary of International Zeolite Conference, vol.170, Elsevier, pp.1236–43

Authors and Affiliations

Matias Alvear[1] · Christoph Schmidt[1] · Ole Reinsdorf[1] · Edgard Lebron-Rodrigez[2] · Abdullah Al Abdulghani[3] · Ive Hermans[2,3] · Markus Peurla[4] · Mika Lastusaari[5] · Kari Eränen[1] · Dmitry Yu. Murzin[1] · Narendra Kumar[1] · Tapio Salmi[1]

✉ Tapio Salmi
tapio.salmi@abo.fi

[1] Laboratory of Industrial Chemistry and Reaction Engineering (TKR), Åbo Akademi University, Åbo/Turku, Finland

[2] Department of Chemical and Biological Engineering, University of Wisconsin-Madison, Madison, WI, USA

[3] Department of Chemistry, University of Wisconsin-Madison, Madison, WI, USA

[4] Institute of Biomedicine, University of Turku, Åbo/Turku, Finland

[5] Intelligent Materials Chemistry Group, Department of Chemistry, University of Turku, Åbo/Turku, Finland